TOXICOLOGICAL SCIENCES **64,** 111–121 (2001)

Dosimetry Modeling of Inhaled Formaldehyde: Binning Nasal Flux Predictions for Quantitative Risk Assessment

J. S. Kimbell,*[,1] J. H. Overton,† R. P. Subramaniam,*[,2] P. M. Schlosser,* K. T. Morgan,*[,3] R. B. Conolly,* and F. J. Miller*

**CIIT Centers for Health Research, P.O. Box 12137, 6 Davis Drive, Research Triangle Park, North Carolina 27709; and †Experimental Toxicology Division, National Health and Environmental Effects Research Laboratory, Office of Research and Development, U.S. Environmental Protection Agency, Research Triangle Park, North Carolina 27711*

Received March 26, 2001; accepted August 4, 2001

Interspecies extrapolations of tissue dose and tumor response have been a significant source of uncertainty in formaldehyde cancer risk assessment. The ability to account for species-specific variation of dose within the nasal passages would reduce this uncertainty. Three-dimensional, anatomically realistic, computational fluid dynamics (CFD) models of nasal airflow and formaldehyde gas transport in the F344 rat, rhesus monkey, and human were used to predict local patterns of wall mass flux (pmol/[mm^2-h-ppm]). The nasal surface of each species was partitioned by flux into smaller regions (flux bins), each characterized by surface area and an average flux value. Rat and monkey flux bins were predicted for steady-state inspiratory airflow rates corresponding to the estimated minute volume for each species. Human flux bins were predicted for steady-state inspiratory airflow at 7.4, 15, 18, 25.8, 31.8, and 37 l/min and were extrapolated to 46 and 50 l/min. Flux values higher than half the maximum flux value (flux median) were predicted for nearly 20% of human nasal surfaces at 15 l/min, whereas only 5% of rat and less than 1% of monkey nasal surfaces were associated with fluxes higher than flux medians at 0.576 l/min and 4.8 l/min, respectively. Human nasal flux patterns shifted distally and uptake percentage decreased as inspiratory flow rate increased. Flux binning captures anatomical effects on flux and is thereby a basis for describing the effects of anatomy and airflow on local tissue disposition and distributions of tissue response. Formaldehyde risk models that incorporate flux binning derived from anatomically realistic CFD models will have significantly reduced uncertainty compared with risk estimates based on default methods.

Key Words: **formaldehyde; nasal passages; nasal airflow; nasal uptake; F344 rat; rhesus monkey; human; regional dosimetry; local dosimetry; computational fluid dynamics.**

People can be exposed to formaldehyde in both occupational and environmental settings, typically at concentrations well below 1 ppm. Formaldehyde is a nasal carcinogen in rodents chronically exposed by inhalation to 6 ppm or higher (Kerns *et al.,* 1983; Monticello *et al.,* 1996). Because epidemiological associations between human cancer incidence and formaldehyde exposure are equivocal (Blair *et al.,* 1990; Collins *et al.,* 1997; Partanen, 1993), the extrapolation of dose and response from laboratory animals to humans is necessary when assessing potential carcinogenic risk in humans exposed to formaldehyde. Since formaldehyde was first shown to be a rat nasal carcinogen (Swenberg *et al.,* 1980), research on respiratory effects of inhaled formaldehyde in laboratory animals has led to several human health risk assessments (Health and Welfare Canada, 1987; U.S. EPA, 1987, 1991). Extrapolations of target tissue dose and tumor response among species have been significant sources of uncertainty in all these assessments.

Uncertainty from interspecies extrapolation of target tissue dose in formaldehyde risk assessments to date arises primarily from an inability to account for both the site- and species-specific patterns of nasal lesions induced by formaldehyde in rats and monkeys. Lesion locations have been correlated with high levels of formaldehyde-induced DNA–protein cross-links (DPX; Casanova *et al.,* 1991, 1994) and with local inspiratory airflow patterns in both species (Morgan *et al.,* 1991). Lesions in rats were confined to the nasal passages but were found as far down in the respiratory tract of monkeys as the carina (Monticello *et al.,* 1989, 1991). These studies imply that local formaldehyde dose plays a major role in determining formaldehyde-induced lesion distributions.

Various metrics have been used to define formaldehyde dose. In the earliest quantitative risk assessments of formaldehyde carcinogenicity, dose was based on exposure concentration in ppm or μg/m^3 (Health and Welfare Canada, 1987; U.S.

This manuscript has been reviewed in accordance with the policy of the National Health and Environmental Effects Research Laboratory, U.S. Environmental Protection Agency, and approved for publication. Approval does not signify that the contents necessarily reflect the views and policies of the Agency, nor does mention of trade names or commercial products constitute endorsement or recommendation for use.

Portions of this data were presented at the annual meeting of the Society for Risk Analysis, December, 1997, Washington, D.C., and at the 37th and 39th annual meetings of the Society of Toxicology, March 1998 and March 2000, Seattle, WA, and Philadelphia, PA.

[1] To whom correspondence should be addressed. Fax: (919) 558-1300. E-mail: kimbell@ciit.org.

[2] Present address: U.S. Environmental Protection Agency, Washington, D.C.

[3] Present address: GlaxoSmithKlein Inc., Research Triangle Park, NC.

EPA, 1987). To decrease the uncertainty associated with interspecies extrapolation of dose, a subsequent risk assessment was based on DPX as a dose metric in pmol/mg DNA (U.S. EPA, 1991). To express the net transport of formaldehyde from inspired air to the air-liquid interface of the nasal walls, wall mass flux in units of mass/(area-time) may be used such as was done for the uptake of inhaled ozone (Overton and Miller, 1988). Formaldehyde wall mass flux as a measure of transport prior to disposition within the body is critical to determining the link between administered doses such as exposure concentrations and target tissue doses or markers of exposure such as DPX. Knowledge of local formaldehyde wall mass flux patterns can also be used to better understand the relative roles that dose and tissue susceptibility play in the disposition of formaldehyde in tissue and responses such as enhanced cell proliferation and tumors.

Unlike rats, monkeys and humans are oronasal breathers. During oronasal and oral breathing, the scrubbing efficiency of the nasal passages is reduced. Breathing route has a significant effect on human pulmonary response from exposure to the highly water soluble gas sulfur dioxide (Adams *et al.,* 1989; Kirkpatrick *et al.,* 1982) and varies during different levels of physical exertion (Niinimaa *et al.,* 1981). Since formaldehyde is water soluble and formaldehyde-induced lesions were observed as far down the respiratory tract as the first bifurcation of the lungs in exposed monkeys, the entire human respiratory tract should be considered for various activity states when studying potential effects of formaldehyde inhalation.

To better understand the roles of anatomy, airflow patterns, and local dose in species-specific nasal toxicity, 3-dimensional, anatomically accurate (i.e., reconstructed from actual cross sections) computer models of airflow and gas transport in the nasal passages of the F344 rat (Kimbell *et al.,* 1993, 1997a), rhesus monkey (Kepler *et al.,* 1998), and human (Subramaniam *et al.,* 1998) were previously developed using computational fluid dynamics (CFD). The rat and monkey CFD models were created to test the hypothesis that species-specific inspiratory airflow patterns drive formaldehyde uptake in the nasal passages and could account for different distribution patterns of nasal lesions in formaldehyde-exposed rats and monkeys. Therefore factors other than anatomy, breathing rates, the diffusivity of formaldehyde in air, and the high solubility and reactivity of formaldehyde in the liquid lining layer were not included in the models. Predictions of local DPX using the CFD models in conjunction with models for the tissue disposition of formaldehyde were in good agreement with experimental measurements in rats (Cohen Hubal *et al.,* 1997; Conolly *et al.,* 2000) and monkeys (Conolly *et al.,* 2000). These results suggest that the exclusion of other factors potentially affecting formaldehyde uptake from inhaled air, such as the presence of other inhaled contaminants, the presence of water vapor, the nasal cycle, and the relative lengths of inspiration and expiration times, did not contribute substantial error to CFD uptake predictions. Local uptake of inhaled formaldehyde estimated by the rat and monkey CFD models correlated with formaldehyde-induced nasal lesion distributions in both species (Kepler *et al.,* 1998; Kimbell *et al.,* 1993, 1997b), providing support for the hypothesis that species-specific airflow patterns play a major role in driving local formaldehyde-induced toxicity.

Recently, CFD simulations of formaldehyde uptake were updated to incorporate improved estimates of uptake conditions at the interface between air and tissue that differentiate between mucus-coated and nonmucus-coated tissue (Kimbell *et al.,* 2001). The updated simulations were used to estimate flux in sites where DPX and cell proliferation rates were measured in formaldehyde-exposed rats and monkeys and to make interspecies comparisons of predicted regional flux such as maximum values and flux in lesion sites (Conolly *et al.,* 2000; Kimbell *et al.,* 2001).

The CFD models can be used to predict formaldehyde flux throughout the entire nasal passages of the rat, monkey, and human at varying airflow rates. At specific sites where DPX formation and formaldehyde-induced cytotoxicity were measured, relationships between flux and these responses can be estimated. These relationships and flux predictions throughout the nose thus allow an interpolation of DPX and cytotoxicity from measurement sites to the rest of the nasal passages in the rat and monkey, and provide a means for estimating these responses locally in the human nasal passages. When coupled with a model for uptake in the human lung, formaldehyde flux and subsequently DPX formation and potential formaldehyde-induced cytotoxicity could be estimated throughout the human respiratory tract for various activity patterns. This information is critical to biologically based modeling of formaldehyde carcinogenicity that can be used to generate human health risk estimates. However, a strategy for incorporating this information into cancer models while retaining local, species-specific variations in these values is needed.

To address this need, the nasal CFD models described by Kimbell *et al.* (2001) were used to partition the surface of the rat, monkey, and human nasal passages into flux bins to obtain quantitative descriptions of species-specific uptake patterns. An individual flux bin is the portion or portions of the tissue surface that receives flux within a specific range of flux values. An average value of flux over each bin surface area is associated with each bin. In addition, the human nasal CFD model was linked to a 1-dimensional (typical-path) dosimetry model of the human respiratory tract to provide a description of local dosimetry and corresponding flux bins throughout the entire respiratory tract for 4 activity states (Overton *et al.,* 2001). Nasal flux predictions in humans were therefore obtained for inspiratory airflow rates that correspond to these activity states.

From correlations of rat nasal flux with formaldehyde-induced cell proliferation and DPX measured in specific sites in the rat, cell proliferation and DPX can be estimated for each flux bin throughout the rat nasal passages and human respiratory tract at a variety of airflow rates. These estimates allow

cell birth and death processes in cancer cell clonal growth modeling to be parametrized for each flux bin in each species, and to capture human activity patterns as well. Aggregating risk for each flux bin would then produce an overall estimate of cancer risk that incorporates species-specific dosimetry patterns.

This article presents flux bins for the rat, monkey, and human nasal passages as zones that, taken together, describe a partitioning of the surface area of the nasal passages of the rat, monkey, and human based on formaldehyde flux. Tables of nasal surface areas and associated flux values are presented for use in incorporating local, species-specific flux variation into formaldehyde risk assessments. Nasal flux for the human is extended from the work described by Kimbell *et al.* (2001) for resting breathing to flow rates corresponding to other activity states including light and heavy exercise.

METHODS

The CFD models of nasal airflow and formaldehyde gas uptake have been described elsewhere in detail (Kepler *et al.,* 1998; Kimbell *et al.,* 1997a, 2001; Subramaniam *et al.,* 1998). In this section we give an outline of model structure and describe the human airflow and uptake simulations needed to approximate human activity patterns. We explain the linkage between the human nasal CFD model and a typical-path model of the human respiratory tract (Overton *et al.,* 2001) and focus on the construction of flux bins into which nasal surface area was partitioned to provide local flux estimates for interspecies extrapolation of dose and response.

Model structure. The rat and monkey CFD models were constructed from tracings of airway perimeters of the right nasal passages from the nostril to the nasopharynx from serial-step sections of embedded tissue specimens as described by Kimbell *et al.* (1993) and Kepler *et al.* (1995). Symmetry between the right and left sides of the rat and monkey nasal passages was assumed. All surface area estimates from the rat and monkey CFD models were therefore doubled to account for both sides of the nasal passages. The human model was constructed from airway tracings of both sides of the nasal passages from the nostril through the nasopharynx from magnetic resonance image scans as described by Subramaniam *et al.* (1998). Since the human CFD model included both sides, a surface area adjustment was not needed for results from this model.

In-house software (Godo *et al.,* 1995) and the finite element mesh preprocessor of the CFD software package FIDAP (Fluent Inc., Lebanon, NH) were used to generate 3-dimensional computational meshes for each nasal geometry (Kepler *et al.,* 1998; Kimbell *et al.,* 1997a; Subramaniam *et al.,* 1998). All meshes were designed to have elements as uniform in shape and size as anatomy allowed. Steady-state, inspiratory airflow was simulated by solving the Navier-Stokes equations of motion numerically using FIDAP and the nasal meshes. Steady-state airflow was assumed to approximate cyclic breathing patterns based on calculation of the Strouhal number, or frequency parameter (Subramaniam *et al.,* 1998). Briefly, unsteady effects may be considered insignificant when the frequency parameter is less than 1 (Pedley, 1977). The Strouhal number, $S = \omega L/u$, where ω, L, and u are the breathing frequency, axial length of the nasal airway, and the average velocity, respectively, is 0.02 in the human, using $\omega = 0.25$ Hz, $L = 11$ cm, and $u = 144$ cm/s, corresponding to a flow rate of 26 l/min and a cross-sectional area of 3 cm^2 (Subramaniam *et al.,* 1998).

Inspiratory rates for steady-state airflow were derived by dividing the amount of inspired air (tidal volume, V_T) by the estimated time involved in inhalation (half the time a breath takes, or (1/2)(1/[breathing frequency, f]). Thus, an inspiratory flow rate was calculated to be 2 V_T f, or twice the minute volume. Minute volumes for the rat and monkey used in this study were estimated to be 0.288 and 2.4 l/min, respectively. Rat and monkey simulations were therefore carried out at 0.576 and 4.8 l/min, respectively (Kimbell *et al.,* 2001), and at various flow rates using the human mesh as described in detail below. Airflow simulation results, consisting of the magnitude and direction of flow predicted at each mesh point, were subsequently used as inputs to the convective-diffusion equation (Bird *et al.,* 1960) representing formaldehyde transport within the nasal passages.

The areas in which formaldehyde-induced nasal squamous cell carcinomas arise in F344 rats are normally lined by respiratory or transitional epithelium (Morgan *et al.,* 1986). These epithelial types frequently respond to injury by transforming to a squamous epithelial type. The readiness with which the squamous epithelial phenotype is induced by injury to the respiratory and transitional epithelia of the nasal airways may account for squamous cell carcinomas arising from them following a carcinogenic insult. In the current study, attention was focused on formaldehyde uptake predicted in regions that are not normally lined by squamous epithelium. Formaldehyde gas is miscible with water and reacts readily with a number of components of nasal mucus (Bogdanffy *et al.,* 1987). Absorption rates of inhaled formaldehyde by the nasal lining were therefore assumed to depend on where the epithelial lining is coated by mucus and where it is not.

The approximate locations of nonsquamous and mucus- and nonmucus-coated epithelia were mapped onto the meshes, and separate conditions for mucus- and nonmucus-coated regions were imposed on the transport rate (flux) of formaldehyde at the interface between air and the airway lining as described by Kimbell *et al.* (2001). Briefly, formaldehyde flux to the nasal surface was assumed to be directly proportional to the air phase concentration of formaldehyde near the wall, with k_{nm} and k_m denoting the constants of proportionality or tissue-phase mass transfer coefficients for nonmucus- and mucus-coated epithelium, respectively. The uptake of inhaled formaldehyde by nonmucus-coated squamous epithelium located in the nasal vestibule of all 3 species was assumed to be similar to uptake determined by Lodén (1986) in experiments measuring formaldehyde transport through human epidermal tissue. An analysis of these measurements provided a mass transfer coefficient of $k_{nm} = 0.41$ cm/s for nonmucus-coated epithelium (Kimbell *et al.,* 2001). A value of 4.7 cm/s for k_m was obtained for all mucus-coated epithelium in all 3 species by fitting the total percentage of nasal uptake predicted by the rat CFD model to 97% as measured by Patterson *et al.* (1986).

Simulations for human activity patterns. Additional simulations were needed to model human activity patterns. Activity patterns consist of various activity states and time durations. The activity states modeled here consisted of sleeping, sitting, and light and heavy exercise and corresponded to cyclic breathing at minute volumes of 7.5, 9, 25, and 50 l/min, respectively (ICRP66, 1994). Nasal airflow patterns during the inspiratory phase of cyclic breathing were approximated by steady-state inspiratory airflow at flow rates equal to twice the cyclic minute volume except at 50 l/min. At 50 l/min, oronasal breathing occurs for most people with approximately 46% of airflow passing through the nasal passages (ICRP66, 1994; Miller *et al.,* 1988). Thus cyclic rates of 7.5, 9, 25, and 50 l/min corresponded to 15, 18, 50, and 46 l/min steady-state, nasal inspiratory flow rates, respectively, in the human CFD model.

CFD airflow and formaldehyde uptake simulations were conducted at 15 and 18 l/min. Airflow simulations at 46 and 50 l/min could not be done since the highest flow rate for which convergence of the flow equations solver could be obtained in this human mesh was 37 l/min. Thus additional simulations were conducted at 7.4, 25.8, and 31.8 l/min and formaldehyde uptake was extrapolated from these results to 46 and 50 l/min (see section below on Nasal Flux Bins).

As described by Kimbell *et al.* (2001), mass balance errors for air (100 × [amount of air entering nostril – amount exiting the distal outlet]/[amount entering nostril]) and inhaled formaldehyde (100 × [amount entering nostril – amount absorbed by airway surfaces – amount exiting distal outlet]/[amount entering nostril]) were calculated. Flux was calculated as the rate of mass transport in the direction perpendicular to the nasal surface per square millimeter of the surface and had units of pmol/(mm^2-h-ppm).

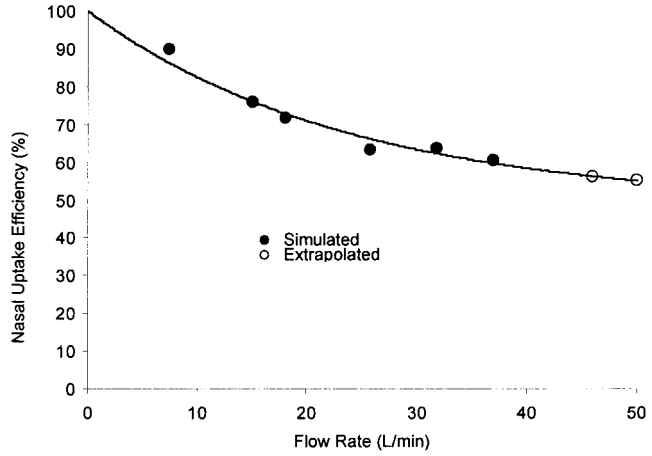

FIG. 1. Extrapolation of human nasal uptake efficiencies to flow rates of 46 and 50 l/min. Fitted curve ($r^2 = 0.97$) is given by *efficiency* = A exp(a × *flow rate*) + B exp(b × *flow rate*), where A = 50.0, B = 50.0, a = -3.00×10^{-4}, and b = -4.25×10^{-2}.

Because airflow and formaldehyde uptake were simulated separately, or uncoupled, errors in mass balance arose separately from these calculations. Errors in mass balance of air were less than 0.4% in all airflow simulations. Mass balance errors associated with simulated formaldehyde uptake from air into tissue ranged from less than 14% for the rat and monkey and for the human at 7.4 and 15 l/min to approximately 27% at the highest human inspiratory flow rates of 31.8 and 37 l/min. In all the CFD simulations, the calculated amount entering the nostrils minus the calculated amount exiting the outlet was greater than the calculated amount absorbed by airway surfaces. As described by Kimbell *et al.* (2001), most of this error occurred when calculating formaldehyde flux to nasal airway surfaces element by element in the finite-element mesh. Flux estimation in directions perpendicular to airway surfaces evidently contributed error to flux calculations for each element of an airway surface region. This error was largest for element-by-element calculation of flux over large, complex nasal surfaces and less for smaller or flatter surfaces such as the nostrils and outlet.

Because the faces of the CFD mesh elements on the nasal airway surface were roughly uniform in shape and size, simulation results were corrected for mass balance errors by evenly distributing the lost mass over the entire nasal surface and adjusting flux values accordingly. For example, in the 15 l/min case where the mass balance error was 13.5%, this correction was calculated as follows:

$$\textit{Corrected flux} = \textit{Raw flux} + \frac{(0.135)(\textit{rate of formaldehyde entering nostrils})}{(\textit{entire nasal surface area})}. \quad (1)$$

All fluxes presented in this study reflect this type of correction and flux estimates for 46 and 50 l/min inspiratory flow rates were extrapolated from flux estimates at lower flow rates that were corrected this way.

Since formaldehyde is highly water soluble and reactive, absorption was assumed to occur only during inspiration. Thus for each breath, flux into nasal passage walls was assumed to be 0 during exhalation. Simulations of formaldehyde uptake in the entire human respiratory tract using a typical-path model during cyclic breathing conditions (Overton *et al.*, 2001) provided further evidence supporting this assumption. In this article, flux values represent an average over the breathing cycle; therefore flux values presented here were derived by halving estimates made using the steady-state inspiratory CFD models, assuming that inspiratory and expiratory phases of the breathing cycle take equal amounts of time.

Linking human nasal CFD and a typical-path lung model. A linkage between formaldehyde uptake simulations using the human nasal CFD model and a typical-path lung model was necessary to provide formaldehyde uptake estimates throughout the human respiratory tract (Overton *et al.*, 2001). To provide this link, the uptake efficiency of the nasal passage compartment of the typical-path model was required to equal that of the nasal CFD model at each of the 4 flow rates. The uptake efficiency of the nasal CFD model was calculated as 100% × (mass of formaldehyde entering nostril - mass exiting outlet)/(mass entering nostril). Uptake efficiencies at 46 and 50 l/min were extrapolated from efficiencies at 7.4, 15, 18, 25.8, 31.8, and 37.0 l/min by empirically fitting a curve to these efficiencies. A good fit was obtained using a curve of the form

$$\textit{efficiency} = \text{A exp}(\text{a} \times \textit{flow rate}) + \text{B exp}(\text{b} \times \textit{flow rate}), \quad (2)$$

where A, B, a, and b were fitted parameters with the constraint that A + B = 100 (Fig. 1). This type of curve fit the simulated efficiencies considerably better than a single exponential. The best fit was obtained ($r^2 = 0.97$) when A = 50.0, B = 50.0, a = -3.00×10^{-4}, and b = -4.25×10^{-2}. As an additional check on the calibration of the typical-path model to the CFD model, average nasal airway surface flux was also computed (see below).

Nasal flux bins. In this section we describe the means by which species-specific, local variation in nasal formaldehyde flux was structured for use in health risk assessments for formaldehyde. A structure was needed so that (1) flux information could be used to generate local dose-response curves for nasal tissue effects and (2) flux predictions from human simulations at different airflow rates would be made at consistent sites.

To address these issues, the portion of the nasal surface of each species that is not normally lined by squamous epithelium was contoured or partitioned by formaldehyde flux into several levels for flux values evenly spaced between 0 and the maximum predicted flux value. A flux bin was defined as the nasal surface area of 1 of these contour levels (Fig. 2). Epithelia that is not normally of the squamous phenotype was identified as the region at risk from formaldehyde-induced carcinogenesis so the region near the nostrils lined by normal squamous epithelium was excluded from this partitioning in all 3 species. As an example, when 3 levels were used to contour flux at 15 l/min in the human (Fig. 2), the first bin contained the amount of nasal surface area where regional flux values fell between 0 and 694 pmol/(mm^2-h-ppm) or 1/3 of the maximum flux of 2082 pmol/(mm^2-h-ppm), the second bin contained the nasal surface

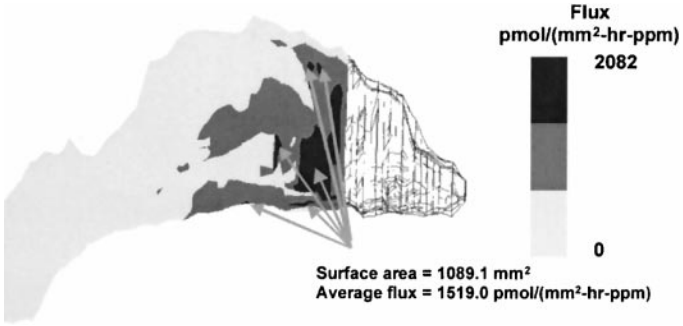

FIG. 2. Illustration of formaldehyde flux bins. Here the nonsquamous-lined portion of the human nasal surface was contoured or partitioned (binned) by formaldehyde flux estimated for a flow rate of 15 l/min into 3 levels (colored light gray, dark gray, and black) for flux values evenly spaced between 0 and 2082 pmol/(mm^2-h-ppm). A flux bin was defined as the nasal surface area of 1 of these levels, such as 1089.1 mm^2 for the black, highest-flux region. An average flux value of 1519.0 pmol/(mm^2-h-ppm) was calculated for this region. Note that the nasal vestibule, to the right, was excluded from the flux binning analysis due to the assumption that this region was lined by squamous epithelium.

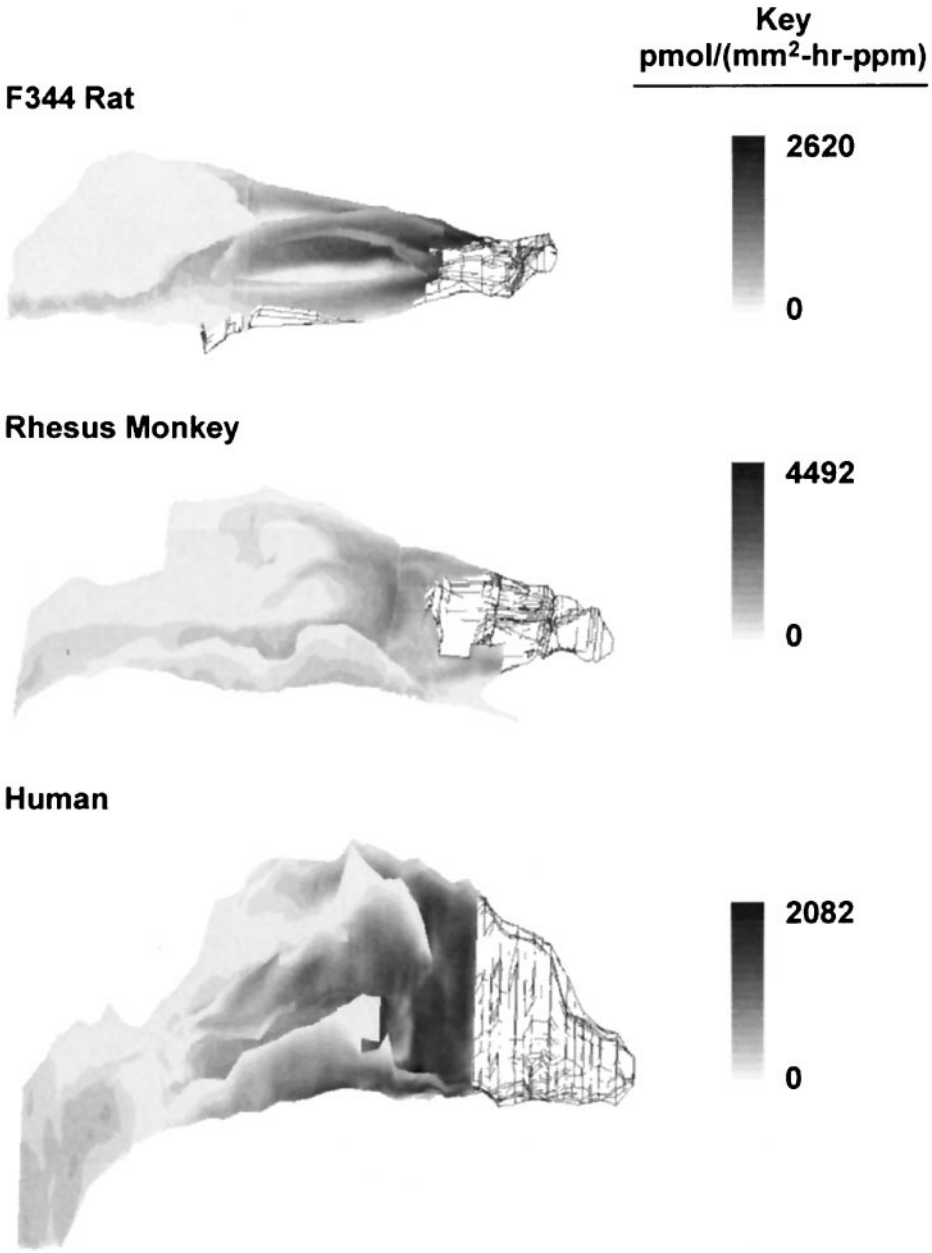

FIG. 3. Illustration of 20 flux bins in each species: right lateral views of formaldehyde flux patterns on the nasal walls of the F344 rat, rhesus monkey, and human. Note different scale for each species-specific flux maximum. See Figure 5 in Kimbell *et al.* (2001) for flux comparison across species using same flux scale. Nostrils are to the right. Black denotes areas of high flux; white denotes areas of low flux except in the nasal vestibule of each species (black outline) that was excluded from the analyses. Each panel shows flux in nonsquamous-lined areas contoured over 20 bins evenly spaced between 0 and the maximum flux value attained in each species. Inspiratory airflow rates were 0.576 l/min in the rat, 4.8 l/min in the monkey, and 15 l/min in the human.

area where flux fell between 694 and 1388 pmol/(mm^2-h-ppm), and the third bin contained the surface area where flux fell between 1388 and 2082 pmol/(mm^2-h-ppm). Each bin was then associated with an average flux value calculated over the surface area of the region defined by that contour level. Average flux values of 307.9, 1004.5, and 1519.0 pmol/(mm^2-h-ppm) and surface areas of 12901.2, 7374.4, and 1089.1 mm^2 were associated with the flux bins in the 3-bin example (Fig. 2).

Using these methods, the nasal walls in the rat, monkey, and human were partitioned into 3, 5, 10, 15, 20, and 25 flux bins. The approximation of predicted flux patterns by flux bins (flux resolution) improved as the number of bins increased, with visible improvement in all 3 species from the use of 3 bins to 20 bins, illustrated for the human by comparing Fig. 2 with the human in Fig. 3. The use of 25 flux bins did not visibly increase the level of flux resolution over 20 bins so 20 bins were used in all subsequent results reported for all 3 species.

In the human, defining flux bins by flux at different flow rates was problematical since flux patterns shifted from flow rate to flow rate. In order for flux predictions from human simulations at different airflow rates to be made at consistent sites, the surface area associated with each bin was based on the 15 l/min CFD simulation and defined to be the same for all other inspiratory

airflow rates. The average flux in the locations defined by the 15 l/min binning procedure was then calculated for each of the simulated inspiratory nasal airflow rates.

Airflow and formaldehyde uptake simulations in the human nasal airways at inspiratory flow rates associated with moderate and heavy exercise exceeded current capabilities for direct computation. To provide flux distribution estimates for these higher flow rates, average flux per bin was extrapolated to the inspiratory nasal airflow rates of 46 and 50 l/min by fitting curves to plots of the average flux per bin versus inspiratory nasal airflow rate for each bin at flow rates of 7.4, 15.0, 18.0, 25.8, 31.8, and 37.0 l/min. Specifically, average flux was assumed to be a function of inspiratory nasal airflow rate. Either a power function of the form

$$flux = a \times (flow\ rate)^b \quad (3)$$

or a rational function of the form

$$flux = (c \times flow\ rate)/(d + flow\ rate) \quad (4)$$

was used to model the functional relationship depending on which equation provided a better fit to the data. Estimates for a, b, c, and d providing the best fit of Equation 3 or Equation 4 to the flux versus flow rate points were obtained using the Levenberg-Marquardt method, a commonly used, nonlinear, least-squares routine (Press *et al.*, 1986) implemented using DeltaGraph Pro (DeltaPoint, Inc., Monterey, CA). The fit producing the higher r^2 (correlation coefficient squared, here representing the fraction of total variation in the data explained by the model) was chosen to represent the relationship between bin-averaged flux and inspired nasal airflow rate for that bin.

Two methods were used to compute average human nasal airway surface flux for comparison with results for the nasal compartment of the typical-path model of Overton *et al.* (2001). At 15 and 18 l/min, the simulations themselves were used to calculate flux averaged in an area-weighted manner over the entire nasal surface. At 46 and 50 l/min, flow rates for which there were no simulations to provide direct calculations, total mass estimated to enter the nostrils was multiplied by the total nasal uptake efficiency estimated for each flow rate to get an estimate of the total mass absorbed at each flow rate. This mass was then divided by the surface area of the entire nasal passages to estimate average nasal airway surface flux.

RESULTS

The maximum formaldehyde wall mass flux estimate averaged over the breathing cycle obtained in the nonsquamous epithelium of each species at twice the minute volume flow rate was 2620 pmol/(mm^2-h-ppm) at 576 ml/min in the rat, 4492 pmol/(mm^2-h-ppm) at 4.8 l/min in the monkey, and 2082 pmol/(mm^2-h-ppm) at 15 l/min in the human (Kimbell *et al.*, 2001). The ranges from 0 to these flux values in the rat, monkey, and human were partitioned into 20 flux bins (Fig. 3), and the surface area was calculated for each flux bin in the CFD models. The amount of nasal surface area where regional flux estimates fell within the specified range defining each bin, along with average flux for that surface area, is given in Tables 1, 2, and 3 for the rat and monkey and for the human at 15 l/min, respectively and in Table 4 for the human at 15, 18, 46, and 50 l/min. In some cases, fluxes within the range of a specific bin were not attained anywhere in the mesh of the nasal surface, thereby producing a 0 surface area for that bin (e.g., Table 2).

TABLE 1
F344 Rat Nasal Surface Area Partitioned by Predicted Formaldehyde Flux

		Nasal surface area	
Flux range	Average flux in bin	Area where flux falls in specified range (mm^2)	% Total nonsquamous
$0 \le$ flux $<$ 131	51	1035	60.8
$131 \le$ flux $<$ 262	190	166	9.7
$262 \le$ flux $<$ 393	325	110	6.4
$393 \le$ flux $<$ 524	456	77	4.5
$524 \le$ flux $<$ 655	588	71	4.2
$655 \le$ flux $<$ 786	718	44	2.6
$786 \le$ flux $<$ 917	858	38	2.2
$917 \le$ flux $<$ 1048	978	32	1.9
$1048 \le$ flux $<$ 1179	1109	27	1.6
$1179 \le$ flux $<$ 1310	1245	21	1.2
$1310 \le$ flux $<$ 1441	1374	20	1.2
$1441 \le$ flux $<$ 1572	1508	17	1.0
$1572 \le$ flux $<$ 1703	1637	18	1.1
$1703 \le$ flux $<$ 1834	1764	13	0.7
$1834 \le$ flux $<$ 1965	1896	10	0.6
$1965 \le$ flux $<$ 2096	2019	3	0.2
$2096 \le$ flux $<$ 2227	2159	1	0.1
$2227 \le$ flux $<$ 2358	2283	$<$ 0.5	$<$ 0.1
$2358 \le$ flux $<$ 2489	2398	$<$ 0.5	$<$ 0.1
$2489 \le$ flux $<$ 2620	2565	$<$ 0.5	$<$ 0.1

Note. Flux range and average flux in bin are given in pmol/[mm^2-h-ppm].

Flux binning provided a means for comparing the distribution of flux among rats, monkeys, and humans at airflow rates equal to their respective resting minute volumes. There was a decreasing gradient of flux from proximal to distal regions in all 3 species. This gradient was predicted to be less steep in humans than in rats or monkeys. A higher percentage of nasal surface area was associated with flux values above the median value in the human at 15 l/min than in the rat at 0.576 l/min or monkey at 4.8 l/min (Fig. 4). Nearly 20% of human nasal surface area was estimated to be associated with flux values above the median at Bin 10, whereas only 5% of rat and less than 1% of monkey nasal surfaces were associated with fluxes higher than the rat and monkey flux medians, respectively.

In the human nasal airways, patterns of predicted nasal surface fluxes shifted distally as the inspiratory flow rate increased (Fig. 5). The proximal-to-distal flux gradient flattened out with increasing inspiratory flow rate, and surface areas predicted to receive moderate levels of formaldehyde flux increased. Maximum flux values in the human were predicted to increase with increasing flow rate (1572, 2082, 2181, 2583, 3086, and 3423 pmol/(mm^2-h-ppm) at flow rates of 7.4, 15.0, 18.0, 25.8, 31.8, and 37.0 l/min, respectively). Human nasal surface areas receiving flux higher than 75% of the maximum flux value were predicted to decrease with increasing flow rate (772, 328, 335, 103, 26, and 10 mm^2 at flow rates of 7.4, 15.0, 18.0, 25.8, 31.8, and 37.0 l/min, respectively). These results are

TABLE 2
Rhesus Monkey Nasal Surface Area Partitioned by Predicted Formaldehyde Flux

Flux range	Average flux in bin	Nasal surface area: Area where flux falls in specified range (mm^2)	Nasal surface area: % Total nonsquamous
$0 \leq$ flux $<$ 225	118	1907	28.4
225 $\leq$ flux $<$ 449	334	1347	20.0
449 $\leq$ flux $<$ 674	558	1137	16.9
674 $\leq$ flux $<$ 898	792	1057	15.7
898 $\leq$ flux $<$ 1123	995	764	11.4
1123 $\leq$ flux $<$ 1348	1228	306	4.5
1348 $\leq$ flux $<$ 1572	1432	140	2.1
1572 $\leq$ flux $<$ 1797	1665	40	0.6
1797 $\leq$ flux $<$ 2021	1901	13	0.2
2021 $\leq$ flux $<$ 2246	2107	7	0.1
2246 $\leq$ flux $<$ 2471	2360	2	$<$ 0.1
2471 $\leq$ flux $<$ 2695	2595	$<$ 0.5	$<$ 0.1
2695 $\leq$ flux $<$ 2920	2840	1	$<$ 0.1
2920 $\leq$ flux $<$ 3144	3022	$<$ 0.5	$<$ 0.1
3144 $\leq$ flux $<$ 3369	3150	$<$ 0.5	$<$ 0.1
3369 $\leq$ flux $<$ 3594	NA[a]	$<$ 0.5	$<$ 0.1
3594 $\leq$ flux $<$ 3818	3647	$<$ 0.5	$<$ 0.1
3818 $\leq$ flux $<$ 4043	NA	$<$ 0.5	$<$ 0.1
4043 $\leq$ flux $<$ 4267	NA	$<$ 0.5	$<$ 0.1
4267 $\leq$ flux $<$ 4492	4382	$<$ 0.5	$<$ 0.1

Note. Flux range and average flux in bin are given in pmol/[mm^2-h-ppm]. NA, not available since there were no surface elements with fluxes in this range.

consistent with increased airflow pushing inhaled gas further into the respiratory tract.

In the human, average flux for each bin was calculated from formaldehyde uptake simulations at 15 and 18 l/min and was extrapolated to 46 and 50 l/min from formaldehyde uptake simulations at 7.4, 15.0, 18.0, 25.8, 31.8, and 37.0 l/min (Table 4). In all cases, r^2 for the best fit relating bin-averaged flux to nasal inspiratory airflow rate was greater than 0.94, and r^2 was greater than 0.98 in 19 of the 20 fits (Fig. 6). Formaldehyde uptake simulations predicted that overall percentage uptake by the human nasal airways decreased with increasing volumetric airflow rate (Fig. 1), implying increased relative uptake in the lower airways. Nasal uptake estimates ranged from 89.9% at 7.4 l/min to 60.5% at 37.0 l/min, with extrapolated values of 56.4% and 55.2% at 46 and 50 l/min, respectively. Formaldehyde flux averaged over the entire human nasal surface was estimated to be 568 and 645 pmol/(mm^2-h-ppm) from uptake simulations at 15 and 18 l/min, respectively and extrapolated to be 1294 and 1376 pmol/(mm^2-h-ppm) at 46 and 50 l/min, respectively.

DISCUSSION

The use of a biologically based modeling approach to risk assessment (Conolly and Andersen, 1991; U.S. EPA, 1996) provides a structure for identifying and quantifying sources of uncertainty. Specific sources of uncertainty can be identified in the framework of biologically based modeling to a far greater extent than can usually be done using default methods. Default methods are meant to be used in the absence of chemical-specific data and are often based on trans-species generalities about anatomical structure, function, physiology, and chemistry. Uncertainty is therefore intrinsic in default methods, and the broad scope of these methods precludes a detailed breakdown of uncertainty sources. The increased ability to identify sources of uncertainty using biologically based modeling does not mean that uncertainty is increased. In fact, informed use of biologically based models in risk assessment represents an inherent reduction in uncertainty because uncertainty sources can be identified, quantified, and made explicit. This is an emphasis of the new cancer risk assessment guidelines recently drafted by the United States Environmental Protection Agency (U.S. EPA, 1996).

Uncertainty in risk estimates based on the use of models such as those presented here arises primarily from the assumptions made about model structures and parameter values used. In many cases, the justification for the assumption or parameter value lowers its contribution to uncertainty; in other cases, sensitivity analyses are necessary to understand effects of the assumption or parameter value on risk estimates. The development and use of CFD models for respiratory tract formalde-

TABLE 3
Human Nasal Surface Area Partitioned by Predicted Formaldehyde Flux at 15 l/min

Flux range	Average flux in bin	Nasal surface area: Area where flux falls in specified range (mm^2)	Nasal surface area: % Total nonsquamous
$0 \leq$ flux $<$ 104	99	650	3.0
104 $\leq$ flux $<$ 208	148	4596	21.5
208 $\leq$ flux $<$ 312	256	2347	11.0
312 $\leq$ flux $<$ 416	359	1671	7.8
416 $\leq$ flux $<$ 520	469	1283	6.0
520 $\leq$ flux $<$ 625	572	1447	6.8
625 $\leq$ flux $<$ 729	675	1318	6.2
729 $\leq$ flux $<$ 833	781	1355	6.3
833$\leq$ flux $<$ 937	885	1282	6.0
937 $\leq$ flux $<$ 1041	989	1233	5.8
1041 $\leq$ flux $<$ 1145	1092	1156	5.4
1145 $\leq$ flux $<$ 1249	1196	915	4.3
1249 $\leq$ flux $<$ 1353	1301	782	3.7
1353 $\leq$ flux $<$ 1457	1402	626	2.9
1457 $\leq$ flux $<$ 1561	1506	378	1.8
1561 $\leq$ flux $<$ 1665	1605	224	1.1
1665 $\leq$ flux $<$ 1769	1705	81	0.4
1769 $\leq$ flux $<$ 1874	1813	15	0.1
1874 $\leq$ flux $<$ 1978	1927	5	$<$ 0.1
1978 $\leq$ flux $<$ 2082	2038	3	$<$ 0.1

Note. Flux range and average flux in bin are given in pmol/[mm^2-h-ppm].

TABLE 4
Bin-Averaged Flux Curve Fit Equations and Predicted Formaldehyde Flux in the Human Nasal Passages

Bin no.	Surface area	Bin-averaged flux curve fits	r^2	Breath-averaged flux (pmol/mm^2-h-ppm) 15 l/min[a] (7.5 l/min)[c]	18 l/min[a] (9 l/min)[c]	46 l/min[a,b] (50 l/min)[c]	50 l/min[a,b] (25 l/min)[c]
1	649.8	$y = 1.9477 \times ^{1.7281}$	0.987	99	133	728	841
2	4595.6	$y = 2.3449 \times ^{1.7822}$	0.996	148	199	1078	1251
3	2347.3	$y = 7.0206 \times ^{1.5552}$	0.995	256	333	1353	1540
4	1670.6	$y = 16.655 \times ^{1.3521}$	0.990	359	451	1475	1651
5	1283.1	$y = 33.615 \times ^{1.1946}$	0.989	469	576	1629	1800
6	1446.9	$y = (15356\ x)/(190.42 + x)$	0.995	572	683	1494	1597
7	1318.1	$y = (8757.1\ x)/(84.794 + x)$	0.996	675	788	1540	1624
8	1354.8	$y = (6472.3\ x)/(48.551 + x)$	0.997	781	893	1575	1642
9	1281.8	$y = (5183.3\ x)/(29.644 + x)$	0.999	885	988	1576	1627
10	1232.7	$y = (4595.3\ x)/(20.153 + x)$	0.999	989	1086	1598	1638
11	1156.2	$y = (4437.9\ x)/(15.605 + x)$	0.998	1092	1184	1657	1691
12	914.7	$y = (4261.9\ x)/(11.639 + x)$	0.996	1196	1281	1701	1729
13	781.6	$y = (4296.6\ x)/(9.5759 + x)$	0.994	1301	1384	1778	1803
14	625.7	$y = 1171.9 \times ^{0.31453}$	0.994	1402	1479	1954	2006
15	378.1	$y = 1421.5 \times ^{0.27090}$	0.994	1506	1576	2005	2051
16	224.4	$y = 1562.7 \times ^{0.26043}$	0.994	1605	1682	2118	2165
17	80.7	$y = (4740.7\ x)/(5.6954 + x)$	0.996	1705	1793	2109	2128
18	14.7	$y = (5136.6\ x)/(6.2772 + x)$	0.991	1813	1905	2260	2282
19	4.6	$y = (6079.4\ x)/(8.8078 + x)$	0.999	1927	2027	2551	2585
20	3.3	$y = (5490.5\ x)/(5.8855 + x)$	0.939	2038	2147	2434	2456

Note. Surface area given in mm^2. Bin-averaged flux curve fits, inspiratory flux only. Each bin has a range of fluxes; the flux value associated with each bin is the area-weighted average flux over the surface area within the bin; fits are to steady-state inspiratory flux values *not* averaged over a breath; y, bin-averaged inspiratory flux in pmol/(mm^2-h-ppm); x, flow rate in l/min; r^2, square of the correlation coefficient between the bin-averaged fluxes and the regression fit.

[a]Steady-state inspiratory airflow rate in nasal airways.

[b]Extrapolated from lower inspiratory flow rates (7.4, 15, 18, 25.8, 31.8, and 37 l/min) using bin-averaged flux curve fit formulas and then dividing by 2 to obtain the estimated breath-averaged value.

[c]Minute volume for cyclic flow.

hyde uptake required a number of assumptions to be made regarding simulation, parameter estimation, and anatomical factors (Kimbell *et al.*, 2001). Model results may be sensitive to several of these factors. The relative contribution to uncertainty of these particular factors is discussed below.

Sources of uncertainty for which sensitivity analyses are appropriate include the use of individual rat, primate, and human nasal anatomies as representative of the general population, the estimation of the distributions of nonsquamous epithelia and mucus- and nonmucus-coated nasal regions in the human, and the number of flux bins used. Quantification of anatomical sources of uncertainty involves determining the extent to which normal variation in these model inputs affects flux estimates. To include variation in nasal anatomy, new models based on a variety of individuals need to be developed and effects on regional flux studied. To determine the location, surface area, and thickness of human nasal epithelial types, detailed mapping using light microscopy on step-sectioned human specimens could be conducted. Analyses to determine the sensitivity of flux resolution to the number of bins used are needed. The methods described here are not limited to a specific number of bins and could be used to conduct these analyses.

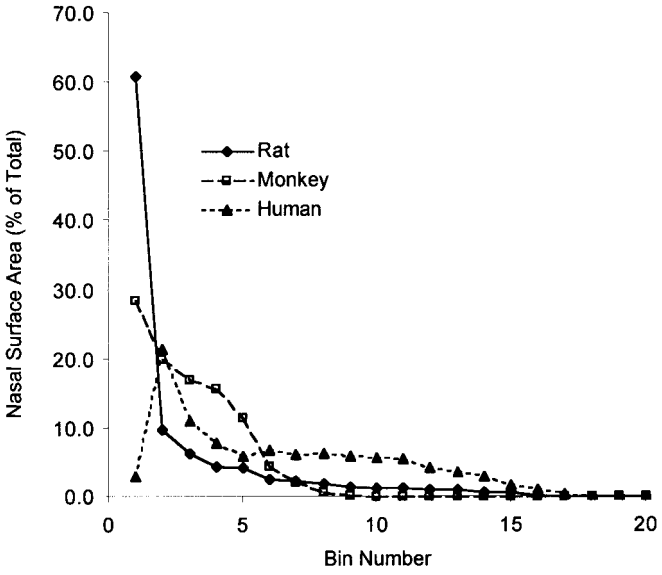

FIG. 4. Allocation of nasal surface area to flux bins for the rat, monkey, and human. Low bin numbers are associated with low flux values. Inspiratory airflow rates were 0.576 l/min in the rat, 4.8 l/min in the monkey, and 15 l/min in the human.

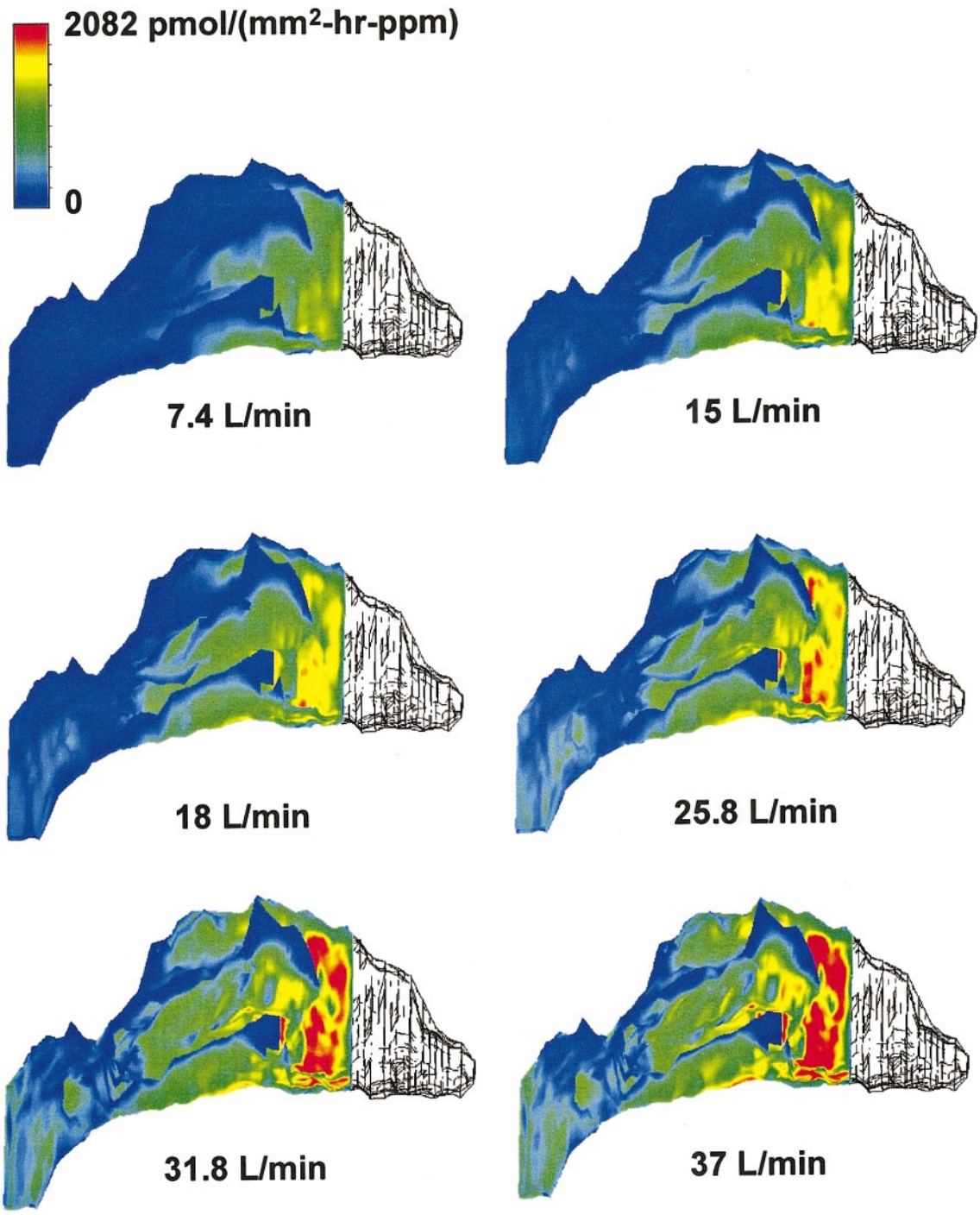

FIG. 5. Airflow rate effects on predicted formaldehyde uptake in the human nasal passages. Right lateral view of human computational fluid dynamics model showing predicted flux over the nonsquamous-lined nasal surface. Red denotes flux values in excess of 2082 pmol/(mm^2-h-ppm), the maximum flux value obtained at 15 l/min.

The values of mass transfer coefficients used in the boundary conditions for simulations of formaldehyde uptake were based on a single estimate of the thickness of the squamous epithelium. Since this thickness is likely to vary among species, simulations using the monkey CFD model were conducted with a 3-fold higher estimate of squamous epithelial thickness. Local fluxes in mucus-coated regions changed by less than 5% (Kimbell *et al.*, 2001). Thus contributions to uncertainty from a lack of knowledge of squamous epithelial thickness in humans are assumed to be low.

Differences between human nasal airways fluxes extrapolated to 46 and 50 l/min from lower flow rates and nasal fluxes

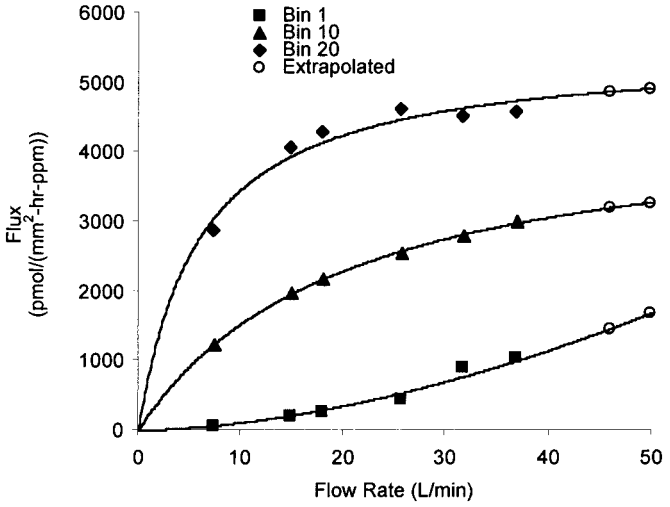

FIG. 6. Three examples of the extrapolation in the human of average flux for each of 20 bins to flow rates of 46 and 50 l/min. Average flux for Bins 1, 10, and 20 (square, triangle, and diamond symbols, respectively) was calculated from formaldehyde uptake simulations at 7.4, 15.0, 18.0, 25.8, 31.8, and 37.0 l/min and extrapolated to 46 and 50 l/min using curve fits (see Table 4). Fitted curves shown here are as follows: Bin 1, *average flux* = 1.9477 (*flow rate*) $^{1.7281}$, r^2 = 0.987; Bin 10, *average flux* = (4595.3 × *flow rate*)/(20.153 + *flow rate*), r^2 =.999; Bin 20, *average flux* = (5490.5 × *flow rate*)/(5.8855 + *flow rate*), r^2 = 0.939.

actually attained in reality at 46 and 50 l/min could arise from variations in nasal airflow patterns, particularly the onset of turbulence (Subramaniam *et al.*, 1998). The transition to turbulence could alter the relationship between uptake and flow rate predicted here. That no such alteration takes place is 1 of the assumptions made in the extrapolations of uptake efficiency and average flux per flux bin from lower to higher flow rates. More research on the effects of turbulence on inhaled gas uptake is needed to address this issue.

Interspecies extrapolation of dose and response has been a significant source of uncertainty in all formaldehyde cancer risk assessments to date. Site-specific nasal lesions observed in species-specific patterns suggest that significant local, species-specific variations in formaldehyde uptake exist. Preliminary studies using 2-stage clonal growth models showed that cancer risk estimates in the rat were sensitive to the predicted local distribution of formaldehyde flux (Kimbell, 1998).

The research described here responds to the general recognition that human health risk assessments should account for interspecies differences in local dosimetry. A number of recent studies have used regional nasal airflow and flux predictions in tissue disposition modeling to strengthen extrapolations of dose and response across species (Andersen *et al.*, 1999; Bogdanffy *et al.*, 1999; Bush *et al.*, 1998; Frederick *et al.*, 1998). The use of the flux-binning approach described here to incorporate local flux predictions into risk assessments captures the role of anatomy and inspiratory airflow patterns in determining site-specific flux from air into tissue. Since flux predicted by the CFD models is a linear function of inhaled concentration (Kimbell *et al.*, 1997b), and since cytotoxicity and DPX are nonlinear with respect to inhaled concentration (Casanova and Heck, 1987; Casanova *et al.*, 1989, 1991, 1994; Monticello *et al.*, 1996), the relationships between flux and responses such as cytotoxicity and DPX formation are nonlinear. Therefore, local variations in flux due to nasal anatomy can lead to large variations in local predictions of potentially adverse effects. Formaldehyde risk models that incorporate flux binning derived from anatomically realistic CFD models will be significantly more accurate, (i.e., less uncertain) than risk estimates based on default methods that do not specifically consider interspecies differences in airway anatomy.

ACKNOWLEDGMENTS

The authors would like to thank CIIT member companies and the American Chemistry Council for supporting this research, Matthew Godo, the technical support staff at Fluent, Inc., Anna Georgieva, Annie Jarabek, Elena Kenyon, Bahman Asgharian, the Formaldehyde Peer Review Workshop Participants assembled by Health Canada in collaboration with the U.S. EPA for research discussions, and Barbara Kuyper for editorial assistance.

REFERENCES

Adams, W. C., Schelegle, E. S., and Shaffrath, J. D. (1989). Oral and oronasal breathing during continuous exercise produce similar responses to ozone inhalation. *Arch. Environ. Health* **44,** 311–316.

Andersen, M. E., Sarangapani, R., Frederick, C. B., and Kimbell, J. S. (1999). Dosimetric adjustment factors for methyl methacrylate derived from a steady-state analysis of a physiologically based clearance-extraction model. *Inhal. Toxicol.* **11,** 899–926.

Bird, R. B., Stewart, W. E., and Lightfoot, E. N. (1960). *Transport Phenomena*. Wiley and Sons, New York.

Blair, A., Saracci, R., Stewart, P. A., Hayes, R. B., and Shy, C. (1990). Epidemiological evidence on the relationship between formaldehyde exposure and cancer. *Scand. J. Work. Environ. Health* **16,** 381–393.

Bogdanffy, M. S., Morgan, P. H., Starr, T. B., and Morgan, K. T. (1987). Binding of formaldehyde to human and rat nasal mucus and bovine serum albumin. *Toxicol. Lett.* **38,** 145–154.

Bogdanffy, M. S., Sarangapani, R., Plowchalk, D. R., Jarabek, A., and Andersen, M. E. (1999). A biologically based risk assessment for vinyl acetate-induced cancer and noncancer inhalation toxicity. *Toxicol. Sci.* **51,** 19–35.

Bush, M. L., Frederick, C. B., Kimbell, J. S., and Ultman, J. S. (1998). A CFD-PBPK hybrid model for simulating gas and vapor uptake in the rat nose. *Toxicol. Appl. Pharmacol.* **150,** 133–145.

Casanova, M., Deyo, D. F., and Heck, H. d'A. (1989). Covalent binding of inhaled formaldehyde to DNA in the nasal mucosa of Fischer 344 rats: Analysis of formaldehyde and DNA by high-performance liquid chromatography and provisional pharmacokinetic interpretation. *Fundam. Appl. Toxicol.* **12,** 397–417.

Casanova, M., and Heck, H. d'A. (1987). Further studies of the metabolic incorporation and covalent binding of inhaled [^{3}H]- and [^{14}C]formaldehyde in Fischer 344 rats: Effects of glutathione depletion. *Toxicol. Appl. Pharmacol.* **89,** 105–121.

Casanova, M., Morgan, K. T., Gross, E. A., Moss, O. R., and Heck, H. d'A. (1994). DNA-protein cross-links and cell replication at specific sites in the nose of F344 rats exposed subchronically to formaldehyde. *Fundam. Appl. Toxicol.* **23,** 525–536.

Casanova, M., Morgan, K. T., Steinhagen, W. H., Everitt, J. I., Popp, J. A., and Heck, H. d'A. (1991). Covalent binding of inhaled formaldehyde to DNA in the respiratory tract of rhesus monkeys: Pharmacokinetics, rat-to-monkey

interspecies scaling, and extrapolation to man. *Fundam. Appl. Toxicol.* **17,** 409–428.

Cohen Hubal, E. A., Schlosser, P. M., Conolly, R. B., and Kimbell, J. S. (1997). Comparison of inhaled formaldehyde dosimetry predictions with DNA-protein cross-link measurements in the rat nasal passages. *Toxicol. Appl. Pharmacol.* **143,** 47–55.

Collins, J. J., Acquavella, J. F., and Esmen, N. A. (1997). An updated meta-analysis of formaldehyde exposure and upper respiratory cancers. *J. Occup. Environ. Med.* **39,** 639–651.

Conolly, R. B. and Andersen, M. E. (1991). Biologically based pharmacodynamic models: Tools for toxicological research and risk assessment. *Annu. Rev. Pharmacol. Toxicol.* **31,** 503–523.

Conolly, R. B., Lilly, P. D., and Kimbell, J. S. (2000). Simulation modeling of the tissue disposition of formaldehyde to predict nasal DNA-protein cross-links in F344 rats, rhesus monkeys, and humans. *Environ. Health Perspect.* **108**(Suppl.), 919–924.

Frederick, C. B., Bush, M. L., Lomax, L. G., Black, K. A., Finch, L., Kimbell, J. S., Morgan, K. T., Subramaniam, R. P., Morris, J. B., and Ultman, J. S. (1998). Application of a hybrid computational fluid dynamics and physiologically-based inhalation model for interspecies dosimetry extrapolation of acidic vapors in the upper airways. *Toxicol. Appl. Pharmacol.* **152,** 211–231.

Godo, M. N., Morgan, K. T., Richardson, R. B., and Kimbell, J. S. (1995). Reconstruction of complex passageways for simulations of transport phenomena: Development of a graphical user interface for biological applications. *Comp. Meth. Prog. Biomed.* **47,** 97–112.

Health and Welfare Canada (1987). *Exposure Guidelines for Residential Indoor Air Quality. A Report of the Federal-Provincial Advisory Committee on Environmental and Occupational Health.* Environmental Health Directorate, Health Protection Branch, Communications Directorate, Department of National Health and Welfare, Ottawa.

ICRP66 (1994). Human Respiratory Tract Model for Radiological Protection. In *Annals of the ICRP*, Vol. 24(1–3). ICRP Publication 66. International Commission on Radiological Protection. Elsevier Science, Tarrytown, NY.

Kepler, G. M., Joyner, D. R., Fleishman, A., Godo, M. N., Richardson, R. B., Gross, E. A., Morgan, K. T., and Kimbell, J. S. (1995). Method for obtaining accurate geometrical coordinates of nasal airways for computer dosimetry modeling and lesion mapping. *Inhal. Toxicol.* **7,** 1207–1224.

Kepler, G. M., Richardson, R. B., Morgan, K. T., and Kimbell, J. S. (1998). Computer simulation of inspiratory nasal airflow and inhaled gas uptake in a rhesus monkey. *Toxicol. Appl. Pharmacol.* **150,** 1–11.

Kerns, W. D., Pavkov, K. L., Donofrio, D. J., Gralla, E. J., and Swenberg, J. A. (1983). Carcinogenicity of formaldehyde in rats and mice after long-term inhalation exposure. *Cancer Res.* **43,** 4382–4392.

Kimbell, J. S. (1998). Sensitivity of risk estimates in F344 rats to regional nasal formaldehyde flux predictions. *Toxicologist* **42,** 299.

Kimbell, J. S., Godo, M. N., Gross, E. A., Joyner, D. R., Richardson, R. B., and Morgan, K. T. (1997a). Computer simulation of inspiratory airflow in all regions of the F344 rat nasal passages. *Toxicol. Appl. Pharmacol.* **145,** 388–398.

Kimbell, J. S., Gross, E. A., Joyner, D. R., Godo, M. N., and Morgan, K. T. (1993). Application of computational fluid dynamics to regional dosimetry of inhaled chemicals in the upper respiratory tract of the rat. *Toxicol. Appl. Pharmacol.* **121,** 253–263.

Kimbell, J. S., Gross, E. A., Richardson, R. B., Conolly, R. B., and Morgan. K. T. (1997b). Correlation of regional formaldehyde flux predictions with the distribution of formaldehyde-induced squamous metaplasia in F344 rat nasal passages. *Mut. Res.* **380,** 143–154.

Kimbell, J. S., Subramaniam, R. P., Gross, E. A., Schlosser, P. M., and Morgan, K. T. (2001). Dosimetry modeling of inhaled formaldehyde: Comparisons of local flux predictions in the rat, monkey, and human nasal passages. *Toxicol. Sci.* **64,** 100–110.

Kirkpatrick, M. B., Sheppard, D., Nadel, J. A., and Boushey, H. A. (1982). Effect of the oronasal breathing route on sulfur dioxide-induced bronchoconstriction in exercising asthmatic subjects. *Am. Rev. Respir. Dis.* **125,** 627–631.

Lodén, M. (1986). The *in vitro* permeability of human skin to benzene, ethylene glycol, formaldehyde, and n-hexane. *Acta Pharmacol. Toxicol.* **58,** 382–389.

Miller, F. J., Martonen, T. B., Menache, M. G., Graham, R. C., Spektor, D. M., and Lippmann, M. (1988). Influence of breathing mode and activity level on the regional deposition of inhaled particles and implications for regulatory standards. *Ann. Occup. Hyg.* **32**(Suppl.), 3–10.

Monticello, T. M., Miller, F. J., and Morgan, K. T. (1991). Regional increases in rat nasal epithelial cell proliferation following acute and subchronic inhalation of formaldehyde. *Toxicol. Appl. Pharmacol.* **111,** 409–421.

Monticello, T. M., Morgan, K. T., Everitt, J. I., and Popp, J. A. (1989). Effects of formaldehyde gas on the respiratory tract of rhesus monkeys: Pathology and cell proliferation. *Am. J. Pathol.* **134,** 515–527.

Monticello, T. M., Swenberg, J. A., Gross, E. A., Leininger, J. R., Kimbell, J. S., Seilkop, S., Starr, T. B., Gibson, J. E., and Morgan, K. T. (1996). Correlation of regional and nonlinear formaldehyde-induced nasal cancer with proliferating populations of cells. *Cancer Res.* **56,** 1012–1022.

Morgan, K. T., Jiang, X. Z., Starr, T. B., and Kerns, W. D. (1986). More precise localization of nasal tumors associated with chronic exposure of F-344 rats to formaldehyde gas. *Toxicol. Appl. Pharmacol.* **82,** 264–271.

Morgan, K. T., Kimbell, J. S., Monticello, T. M., Patra, A. L., and Fleishman, A. (1991). Studies of inspiratory airflow patterns in the nasal passages of the F-344 rat and rhesus monkey using nasal molds: Relevance to formaldehyde toxicity. *Toxicol. Appl. Pharmacol.* **110,** 223–240.

Niinimaa, V., Cole, P., Mintz, S., and Shephard, R. J. (1981). Oronasal distribution of respiratory airflow. *Respir. Physiol.* **43,** 69–75.

Overton, J. H., Kimbell, J. S., and Miller, F. J. (2001). Dosimetry modeling of inhaled formaldehyde: The human respiratory tract. *Toxicol. Sci.* **64,** 122–134.

Overton, J. H. and Miller, F. J. (1988). Dosimetry modeling of inhaled toxic reactive gases. In *Air Pollution, the Automobile, and Public Health* (A. Y. Watson, R. R. Bates, and D. Kennedy, Eds.), pp. 367–385. National Academy Press, Washington, D.C.

Partanen, T. (1993). Formaldehyde exposure and respiratory cancer—a meta-analysis of the epidemiologic evidence. *Scand. J. Work. Environ. Health* **19,** 8–15.

Patterson, D. L., Gross, E. A., Bogdanffy, M. S., and Morgan, K. T. (1986). Retention of formaldehyde gas by the nasal passages of F-344 rats. *Toxicologist* **6,** 55.

Pedley, T. J. (1977). Pulmonary fluid dynamics. *Ann. Rev. Fluid Mech.* **9,** 229–274.

Press, W. H., Flannery, B. P., Teukolsky, S. A., and Vetterling, W. T. (1986). *Numerical Recipes,* pp. 523–528. Cambridge University Press, New York.

Subramaniam, R. P., Richardson, R. B., Morgan, K. T., Kimbell, J. S., and Guilmette, R. A. (1998). Computational fluid dynamics simulations of inspiratory airflow in the human nose and nasopharynx. *Inhal. Toxicol.* **10,** 91–120.

Swenberg, J. A., Kerns, W. D., Mitchell, R. E., Gralla, E. J., and Pavkov, K. L. (1980). Induction of squamous cell carcinomas of the rat nasal cavity by inhalation exposure to formaldehyde vapor. *Cancer Res.* **30,** 3398–3402.

U.S. EPA (1987). Assessment of health risks to garment workers and certain home residents from exposure to formaldehyde. Office of Pesticides and Toxic Substances, U.S. Environmental Protection Agency, Washington, D.C.

U.S. EPA (1991). Formaldehyde risk assessment update—Final draft. Office of Toxic Substances, U.S. Environmental Protection Agency, Washington, D.C.

U.S. EPA (1996). Proposed guidelines for carcinogen risk assessment: Notice of availability and opportunity to comment. *61 Fed. Regist.,* 17960–18011.